RSC Advances

PAPER

View Article Online
View Journal | View Issue

Cite this: *RSC Adv.*, 2022, **12**, 10924

Influence of zirconia addition in TiO_2 and TiO_2–CeO_2 aerogels on the textural, structural and catalytic properties of supported vanadia in chlorobenzene oxidation

Chiraz Gannoun, *[a] Abdelhamid Ghorbel[b] and Eric M. Gaigneaux [c]

Received 24th November 2021
Accepted 2nd March 2022

DOI: 10.1039/d1ra08611a

rsc.li/rsc-advances

This paper studies the effect of the direct incorporation of ZrO_2 in TiO_2 and TiO_2–CeO_2 aerogel supports prepared by sol–gel route on the physico–chemical and catalytic properties of supported vanadia catalysts in the total oxidation of chlorobenzene. The obtained catalysts have been characterized by means of ICP-AES, N_2 adsorption–desorption at 77 K, XRD, XPS, H_2-TPR and NH_3-TPD. The results revealed that Zr-doped V_2O_5 based catalyst is beneficial for the improvement of catalytic properties in chlorobenzene total oxidation. In particular, in the absence of cerium groups, this beneficial effect is correlated with the better acidic properties or/and the stabilization of the V_2O_5 active phase in a higher oxidation state. However, in the case of cerium rich catalyst, this positive effect is much stronger thanks to the enhanced redox properties of V_2O_5/TiO_2–CeO_2–ZrO_2.

1. Introduction

Vanadia based TiO_2 materials constitute a very important class of catalytic materials resistant against chlorinated volatile organic compounds (Cl-VOCs) released in the atmosphere.[1–5] The latter have been considered to be very toxic, carcinogenic and environmentally persistent organic pollutants.[3,6,7] The catalytic destruction of chlorinated VOCs to CO_x, H_2O, HCl and Cl_2 appears as a very promising solution since it allows destroying these pollutants without deactivation of V_2O_5/TiO_2 catalysts by chlorine poisoning on their surfaces.[3]

Besides, we have demonstrated that the direct incorporation of cerium species in the TiO_2 aerogel support prepared by the sol gel route has generated great interest in the catalytic performances of the V_2O_5/TiO_2 catalyst in the total oxidation of chlorobenzene.[8] The success of the use of cerium oxide as a promoter of the V_2O_5/TiO_2 material is due to its oxygen storage and reduction/oxidation properties.[9–11] In fact, labile oxygen vacancies and bulk oxygen species with relatively high mobility are easily formed during the redox shift between Ce^{3+} and Ce^{4+} under oxidizing and reducing conditions. The mechanism of the oxidation reactions of Cl-VOCs over ceria is usually considered to be of the redox or Mars and van Krevelen type. The key step of this mechanism is that CeO_2 supplies active oxygen to the vanadium species that are reduced during the catalytic reaction.[8]

However, the capabilities of the redox couple Ce^{4+}/Ce^{3+} could be strongly enhanced if other elements are introduced into the CeO_2 lattice. Among various elements, the introduction of zirconium in the lattice of CeO_2 is particularly effective in the enhancement of the storage/release capacity and redox properties of CeO_2.[12,13]

On the other hand, the combined TiO_2–ZrO_2 mixed oxide has also attracted considerable attention recently as active catalyst as well as support for a wide variety of catalytic applications.[14–20] In fact, it is established in the literature that mixing these two dissimilar oxides could lead to totally different physico–chemical properties and catalytic behavior since they are liable to form new stable compounds.[21] Such advanced titania–zirconia mixed oxides not only take advantage of both TiO_2 (active catalyst and support) and ZrO_2 (acid–base properties), but also extend their application through the generation of new catalytic sites due to a strong interaction between them.[21] In fact, the facile formation of zirconium titanate ($ZrTiO_4$) compound between ZrO_2 and TiO_2 allows excellent catalytic properties for various reactions.[21]

Therefore, given the favorable characteristics of zirconia, the aim of this work is to study the effect of the direct incorporation of ZrO_2 in TiO_2 and TiO_2–CeO_2 aerogel supports prepared by sol–gel route on the physico–chemical and catalytic properties of supported vanadia catalysts in the total oxidation of chlorobenzene.

To determine the physico–chemical properties of various samples elaborated, different characterization techniques

[a]*Centre National des Recherches en Sciences des Matériaux (CNRSM), Technopôle, Borj Cedria, BP73, 8027 Soliman, Tunisia. E-mail: gannoun.chiraz@gmail.com*
[b]*Laboratoire de Chimie des Matériaux et Catalyse, Département de Chimie, Faculté des Sciences de Tunis, Campus Universitaire, 2092 El Manar Tunis, Tunisia*
[c]*Université Catholique de Louvain, Institute of Condensed Matter and Nanosciences (IMCN), Division "Molecular Chemistry, Materials and Catalysis (MOST)", Place Louis Pasteur 1 L4.01.09, B-1348 Louvain-la-Neuve, Belgium*

namely, BET surface area, inductively coupled plasma-atomic emission spectroscopy (ICP-AES), X-ray diffraction (XRD), temperature-programmed reduction (TPR) with H_2, temperature-programmed desorption of ammonia (NH_3-TPD) and *in situ* diffuse reflectance infrared spectroscopy (DRIFTS) were employed.

2. Experimental

2.1 Elaboration of catalysts

TiO_2, TiO_2–ZrO_2, TiO_2–CeO_2 and TiO_2–CeO_2–ZrO_2 supports were prepared *via* sol–gel method as follows: titanium(IV) isopropoxide (Aldrich, 98%), as precursor, with anhydrous ethanol (Aldrich, 98%), as solvent, was chemically modified by adding acetylacetone (Fluka, 99%) according to a molar ratio acetylacetone/Ti = 1 in order to control hydrolysis and condensation reaction rates. This solution was maintained for 1 h under stirring. To obtain mixed oxides, cerium nitrate (Aldrich, 99.5%) or/and zirconium acetylacetonate (Aldrich, 98%) were added to titanium isopropoxide according to molar ratios Ce/Ti = 0.1 and Zr/Ti = 0.1. Homogenous gels are obtained by hydrolysis and condensation after HNO_3 supply. The amount of distilled water added corresponded to the molar ratio H_2O/Ti = 10. The gels were thereafter transformed into aerogels by drying under supercritical conditions of ethanol (P = 63 bars, T = 243 °C).

Catalysts with nominal vanadia loading of 2 wt% were elaborated by impregnating 2 g of support with 4 ml of an acetone solution of vanadyl acetylacetonate (Fluka, 95%).

The obtained solids are then dried in an oven at 60 °C for 24 h. Finally, catalysts are calcined for 3 h at 500 °C under flowing O_2 (30 ml min^{-1}) and denoted respectively VTi, VTiZr, VTiCe and VTiCeZr.

2.2 Characterization of catalysts

2.2.1 Elemental analysis. The elemental analysis was performed by inductively coupled plasma-atomic emission spectroscopy (ICP-AES) allowing estimating the weight percentage of Ce, Zr and V. These measurements were performed on a Horiba Jobin Yvon apparatus, Model Activa.

2.2.2 N_2 adsorption–desorption at 77 K. Specific surface area and pore volume measurements of the samples were done by N_2 physisorption at 77 K using a Micromeritics ASAP 2020 apparatus. Prior to N_2 physisorption, the samples were outgassed in vacuum during 6 h at 200 °C.

2.2.3 X-ray diffraction (XRD). X-ray diffraction patterns (XRD) were obtained using a MRD PRO PANalytical X'Pert PRO instrument with CuKα radiation (λ = 1.5418 Å) at the rate of 0.02° per s from 5 to 70°.

2.2.4 X-ray photoelectron spectroscopy (XPS). X-ray photoelectron spectra (XPS) were collected on a SSI X probe spectrometer (model SSI 100, Surface Science Laboratories, Mountain View, CA, USA) equipped with a monochromatized AlK_α radiation (1486 eV). The samples powders, pressed in small stainless-steel troughs of 4 mm diameter, were placed on an insulating homemade ceramic carousel. The pressure in the analysis chamber was around 10^{-6} Pa. The angle between the surface normal and the axis of the analyser lens was 55°. The analysed area was approximately 1.4 mm^2 and the pass energy was set at 150 eV. The C 1s peak of carbon has been fixed at 284.8 eV to set the binding energy scale. Data treatment was performed with the CasaXPS program (Casa Software Ltd, UK) and some spectra were decomposed with the least squares fitting routine provided by the software with a Gaussian/Lorentzian (85/15) product function and after subtraction of a non-linear baseline.

2.2.5 Temperature programmed desorption of ammonia (NH_3-TPD). Total acidity was evaluated by temperature-programmed desorption of ammonia (NH_3-TPD) using a quadrupole Balzers QMC 311. Before NH_3 desorption, the samples were pre-treated under He flow (60 ml min^{-1}) at 200 °C for 1 h. NH_3 adsorption was performed under ambient conditions by flowing 0.5% NH_3 in He over the catalyst until saturation and then following the desorption of NH_3 along a temperature-programmed treatment under He from 50 to 500 °C using a heating rate of 10 °C min^{-1}.

2.2.6 Temperature programmed reduction of H_2 (H_2-TPR). Temperature programmed reduction (TPR) experiments were performed in a dynamic apparatus using 5% H_2 in He flowing at 60 ml min^{-1}. Experiments were carried out in the range 30–800 °C. The inlet and outlet gas compositions were measured using a quadrupole mass spectrometer QMC 311 Balzers coupled to the reactor.

2.3 Catalytic test

Catalytic tests were performed with 200 mg of catalyst (200–315 μm) diluted in 800 mg of inactive glass spheres with diameters in the range 315–500 μm in a metallic fixed-bed micro-reactor (PID Eng&Tech, Madrid, Spain) operating at atmospheric pressure and fully monitored by computer. The gas stream was composed of 100 ppm of chlorobenzene, 20 vol% of O_2 and helium as diluting gas to obtain 200 ml min^{-1} (space velocity (VVH) = 37 000 h^{-1}). The reaction was run from 100 to 400 °C by steps of 50 °C. At each temperature investigated, the catalyst was stabilized for 150 min in order to reach steady state. Analysis of the reactants and products was continuously performed by on line gas chromatography (GC). The GC allowed chlorobenzene, O_2, CO, and CO_2 to be quantified and other chlorohydrocarbons to be detected. To calculate the conversion, only the concentrations of the reactants and products measured after stabilization and averaged in a period of time from 100 to 150 minutes were taken into account. The measured performances were accurate within a range of about 1% (in relative) for the conversion of chlorobenzene. Analysis of reactants and products was continuously performed by on line gas chromatography (GC).

3. Results and discussion

3.1 Elemental analysis

Nominal and experimental chemical compositions of the VTi, VTiZr, VTiCe and VTiCeZr samples are compared in Table 1.

Table 1 Element analysis and theoretical composition of VTi, VTiCe, VTiZr and VTiCeZr calcined at 500 °C

	Bulk composition (wt%)			Nominal composition (wt%)		
Catalyst	V	Ce	Zr	V	Ce	Zr
VTi	1.6			1.1		
VTiCe	1.08	14.22		1.1	14.4	
VTiZr	0.99		12.34	1.1		12.4
VTiCeZr	1.02	14.36	12.23	1.1	14.4	12.4

The results indicate a good agreement with the nominal compositions revealing that vanadium, zirconium and cerium were successfully incorporated in the catalysts. The small difference observed may result from inaccuracies in the preparation of the solution of samples for ICP analysis (*ca.* weighing).

3.2 N_2-adsorption–desorption at 77 K

The specific surface areas and pore diameters of TiO_2, TiO_2–ZrO_2, TiO_2–CeO_2 and TiO_2–CeO_2–ZrO_2 aerogel supports (as references) and VTi, VTiZr, VTiCe and VTiCeZr catalysts, calcined at 500 °C are given in Table 2.

All solids are classified as mesoporous materials (pores between 20 and 500 Å) and exhibited specific surface areas higher than industrial TiO_2 such as TiO_2 Degussa P 25, which is a mixture of anatase (70%) and rutile (30%) and which has a surface area of 50 $m^2\ g^{-1}$.[22]

From Table 2, it can be seen that specific surface area of aerogel TiO_2 support synthesized by one-pot sol–gel method appeared to depend only on the cerium content. In fact, CeO_2 is beneficial for the specific surface area of TiO_2 aerogel which increases from 115 $m^2\ g^{-1}$ to 140 $m^2\ g^{-1}$ after incorporation of ceria. However, doping TiO_2 with ZrO_2 allows preserving its pristine specific surface area.

Furthermore, the TiO_2–CeO_2 sample exhibits specific surface area of 140 $m^2\ g^{-1}$. A steady decrease from 140 to 94 $m^2\ g^{-1}$ is observed in the case of TiO_2–CeO_2–ZrO_2 aerogel support. The observed decrease could be due to the penetration of the dispersed zirconium oxide into the pores of TiO_2–CeO_2 support, thereby narrowing its pore diameter and blocking some of the pores.[23]

Table 2 Specific surface areas and mean pore size diameters of supports and catalysts calcined at 500 °C

Sample	Surface area ($m^2\ g^{-1}$)	Pore diameter (Å)
TiO_2	115	80
TiO_2–CeO_2	140	174
TiO_2–ZrO_2	110	137
TiO_2–CeO_2–ZrO_2	94	134
VTi	136	98
VTiCe	141	114
VTiZr	128	139
VTiCeZr	102	95

On the other hand, vanadia based materials were found to display greater or quiet similar specific surface area than TiO_2, TiO_2–ZrO_2, TiO_2–CeO_2 and TiO_2–CeO_2–ZrO_2 supports. It is probable that this effect is due to the elaboration route of vanadia based materials which occurs in two steps.

N_2 adsorption–desorption isotherms at 77 K and pore size distribution curves of Ti, TiCe, TiZr, TiCeZr (as references) and VTi, VTiCe, VTiZr and VTiCeZr are displayed in Fig. 1 and 2, respectively. According to the IUPAC classification,[24] all the samples are characterized by the type IV isotherms (behavior characteristic of mesoporous materials) with hysteresis loops type H1 characteristic of porous materials.[24]

It is clearly seen from the pore size distribution curves of the supports that the modification of TiO_2 by CeO_2, ZrO_2 or CeO_2–ZrO_2 contributes to the enlargement of its pors. The observed increase in the diameter of pores could result from the combination of different pore sizes derived from TiO_2 particle and TiO_2–ZrO_2 or TiO_2–CeO_2 particle on the other hand.[25,26]

After vanadium impregnation, the average pore diameter of TiO_2 increases leading to clear changes in the textural properties. These results could be attributed to the reorganization of TiO_2 crystallites sizes after vanadium impregnation.[27]

In the case of ceria rich catalysts, a decrease in the average pore diameter is observed which could be due to the plugging of the small pores by cerium incorporation.[28] On the contrary, V_2O_5–TiO_2 and V_2O_5–TiO_2–ZrO_2 samples had narrow BJH pore

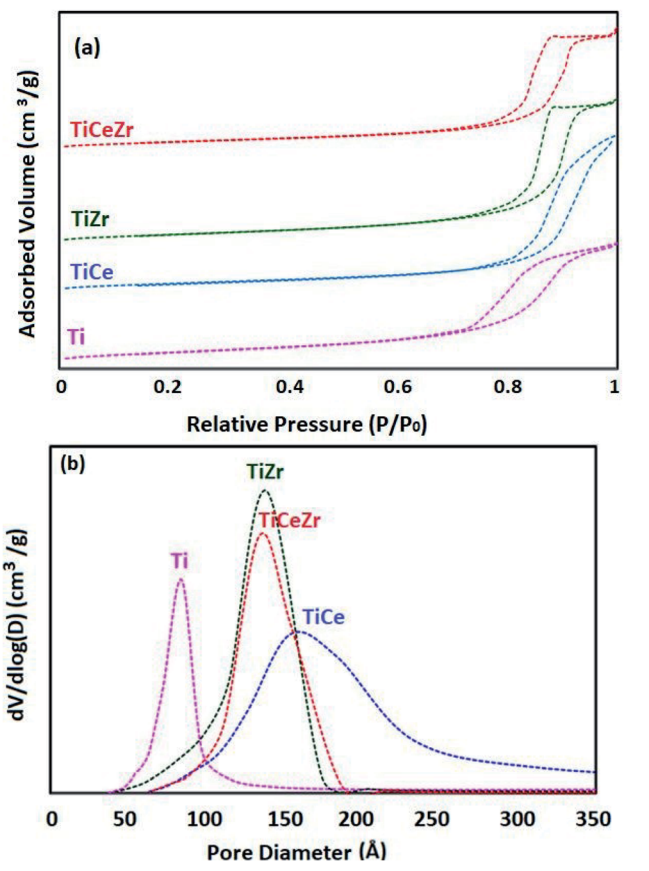

Fig. 1 Textural properties of Ti, TiCe, TiZr and TiCeZr supports: (a) N_2 adsorption–desorption isotherms and (b) pore size distribution curves.

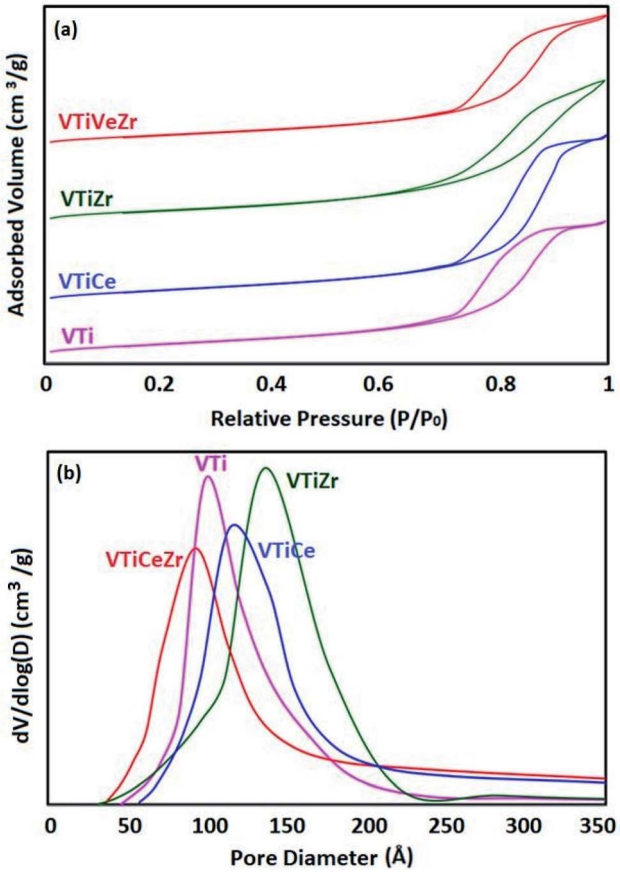

Fig. 2 Textural properties of VTi, VTiCe, VTiZr and VTiCeZr supports: (a) N_2 adsorption–desorption isotherms and (b) pore size distribution curves.

size distributions with diameters centered at 137 Å and 139 Å (Table 2), demonstrating that the doping of zirconium stabilized the mesoporous structure.[29]

3.3 X-ray diffraction

The XRD patterns of VTi, VTiZr, VTiCe and VTiCeZr samples calcined at 500 °C are shown in Fig. 3. Only the broad diffraction lines due to TiO_2 anatase with high cristallinity such as $2\theta = 25°$, 37°, 48° and 53° (PDF-ICDD 21-1272) plus a few peaks belonging to cubic CeO_2 at $2\theta = 28.5°$, 33.3° and 47.4° (PDF 00-034-0394) are identified.

The absence of characteristic lines of ZrO_2 at 2θ values around 28.2°, 31.5°, 38.5°, 50.1°, and 59.8° (ICDD file no. 37-1484) indicates that ZrO_2 is dispersed on TiO_2 and TiO_2–CeO_2 supports.[30]

In addition, the absence of crystalline features of V_2O_5 in the case of the vanadia based materials indicates that vanadium oxide is also dispersed on the surface of the support as vanadates or under the form of small vanadia crystallites undetectable *via* XRD.[31]

3.4 X-ray photoelectron spectroscopy

To investigate the surface composition of the catalysts, XPS measurements were performed. The electron binding energies

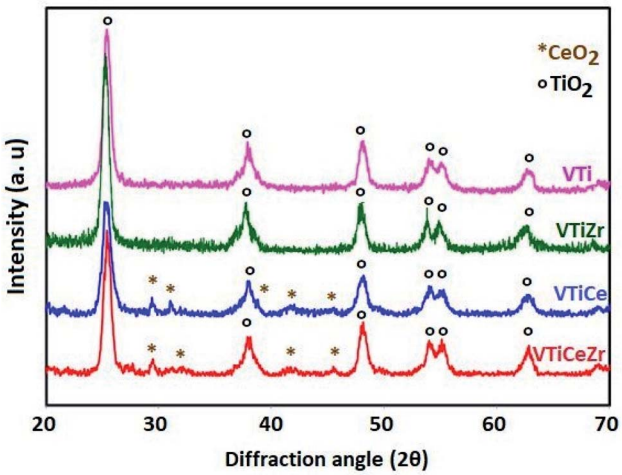

Fig. 3 X-ray diffraction patterns of V_2O_5 based catalysts calcined at 500 °C.

(eV) of Ti 2p, Ce 3d, Zr 3d and V 2p and the surface atomic ratios V/Ti, V/(Ti + Zr),V/(Ti + Ce), V/(Ti + Ce + Zr) are displayed in Table 3.

Table 3 reveals that vanadia spreads more on the surface of TiO_2 and TiO_2–CeO_2 aerogel supports in the absence of zirconium since ratios (V/Ti and V/(Ti + Ce)) diminish when zirconia was incorporated.

The XPS spectra of Ti, Zr, O, Ce and V are presented in Fig. 4. The binding energies of Ti $2p_{3/2}$ and Ti $2p_{1/2}$ were found around 459 and 464 eV for all catalysts. These mentioned results were illustrated in Fig. 4(a). A contribution with binding energies around 182 and 184 eV was detected for samples containing zirconia (Fig. 4(b)). These peaks concerned Zr $3d_{3/2}$ and Zr $3d_{5/2}$. Both Ti 2p and Zr 3d binding energies revealed the presence of 4+ oxidation state for Zr and Ti in the prepared samples.[30,32] However, no indication was observed for metallic Zr (~178 eV).[32]

The spectra of O 1s for the four catalysts were investigated (Fig. 4(c)) and the results showed a main peak located at 530 eV which is typically assigned to the lattice oxygen associated to the metal oxides.[33,34]

Moreover, in the absence of zirconium, a contribution with binding energies around 515 and 517 eV is detected for VTi and VTiCe samples, suggesting that vanadium is a mixture of IV and V oxidation states (Fig. 4(d)).[35] However, doping catalysts with zirconium induces a higher oxidation state of vanadium since only binding energy of V^{5+} is detected (Fig. 4(e)). This result is very promising for the reactivity of V_2O_5 based catalysts in the total oxidation of chlorobenzene since the catalytic response is strongly governed by the higher vanadium oxidation level.[36]

The Ce 3d XPS profiles of VTiCe and VTiZrCe samples treated at 500 °C are shown in Fig. 5. The two samples exhibit peaks due to the presence of both Ce^{4+} and Ce^{3+}, implying that cerium is present at the surface in both 4+ and 3+ oxidation states.[37,38] In particular, the sub-bands labeled with u‴, u″, u, v‴, v″ and v represent the $3d^{10}4f^0$ state of Ce^{4+},[39] and the sub-bands labeled

Table 3 XPS Binding energies and V/X (X = Ti, Ti + Ce, Ti + Zr + Ce) atomic ratios of the VTi, VTiCe, VTiZr and VTiCeZr catalysts calcined at 500 °C

	Binding energy (eV)						Atomic ratio V/X (X = Ti, Ti + Zr, Ti + Ce, Ti + Zr + Ce)			
Catalyst	Ti $2p_{3/2}$	Ce $3d_{5/2}$	Zr $3d_{3/2}$	Zr $3d_{5/2}$	V^{5+} $2p_{3/2}$	V^{4+} $2p_{3/2}$	V/Ti	V/(Ti + Zr)	V/(Ti + Ce)	V/(Ti + Ce + Zr)
VTi	458.2	—		—	517.2	515.9	0.032	—	—	—
VTiCe	458.5	884.5		—	517.3	515.7	—	—	0.077	—
VTiZr	485.3	—	182.0	184.6	517.3	—	—	0.019	—	—
VTiZrCe	485.2		182.2	184.4	517.3	—	—	—	—	0.047

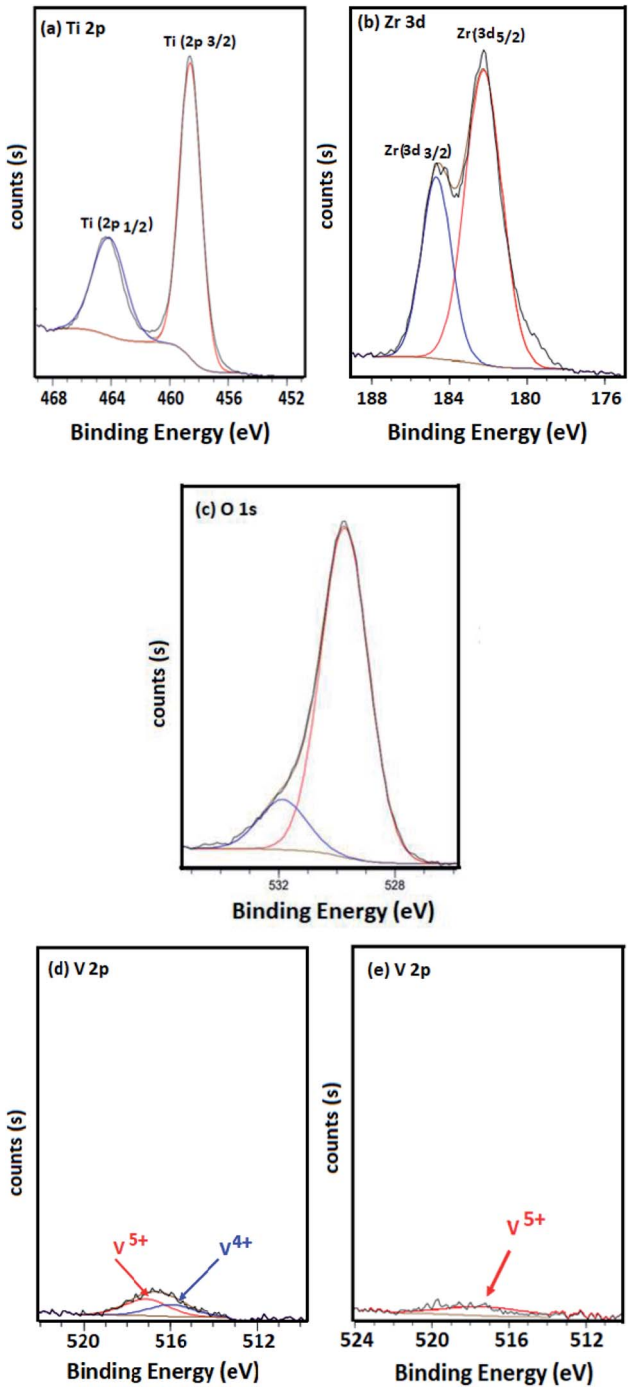

Fig. 4 XPS spectra of elements: (a) Ti, (b) Zr, (c) O, (d) and (e) V.

with u, u°, v' and v° represent the $3d^9 4f^1$ state corresponding to Ce^{3+}.[39] However, the calculated Ce^{3+} fraction of zirconia containing catalyst (61%) is higher than that of VTiCe (37%), indicating that the catalyst with added ZrO_2 contains more Ce^{3+} ions that provides more redox active sites on catalyst surface and plays the role of oxygen vacancy. This result is very promising for the chlorobenzene abatement which is related to the enhanced redox properties.

3.5 NH_3-TPD

To evaluate the acidic properties of the elaborated oxides, NH_3-TPD experiments were undertaken. The obtained profiles are displayed in Fig. 6. The NH_3 desorption profile of VTi shows two unresolved peaks at around 100 °C and 350 °C which are attributed, respectively, to weak and strongly adsorbed ammonia (Fig. 6(a)).[1,40,41] The incorporation of cerium to this sample enhances the total acidity of this catalyst as proven by the increase of the intensities of the two peaks mentioned above[8]

Besides, it seems that the global acidity of V_2O_5/TiO_2 and V_2O_5/TiO_2–CeO_2 materials is influenced by the addition of ZrO_2. In particular, the intensity of the first peak centred at 100 °C increases considerably indicating that zirconium generates a new type of weak acid sites on the surface of V_2O_5/TiO_2 catalyst which could reveal highly beneficial for the catalytic performances of V_2O_5/TiO_2 as discussed in earlier works.[1,42] For VTiCeZr sample, the NH_3-desorption temperatures from weak acid sites are shifted toward higher temperatures reflecting an increase in the strength of the weak acid sites. This result is very promising since the acidity is crucial in the adsorption of the VOCs on its surface.[1]

Furthermore, the introduction of ZrO_2 did not seem to change significantly the peak intensities of strong acidic sites in the case of VTiZr and VTiCeZr materials. However, TPD profile of V_2O_5/TiO_2–CeO_2–ZrO_2 revealed that the strength of strong acid sites was higher than that of V_2O_5/TiO_2–CeO_2 since the NH_3-desorption temperatures shifted toward higher temperatures. Based on literature,[43] strong acid sites which are present on the surface of supports improve the spreading of VO_x active phase and consequently, could favour a better catalytic activity.

3.6 H_2-TPR

The reducibility of zirconium, vanadium and cerium species was examined by H_2-TPR (Fig. 7). The TPR profiles of V_2O_5 based materials exhibit unresolved peaks maximizing at about 491 °C, 474 °C and 441 °C which might be ascribed to the reduction of

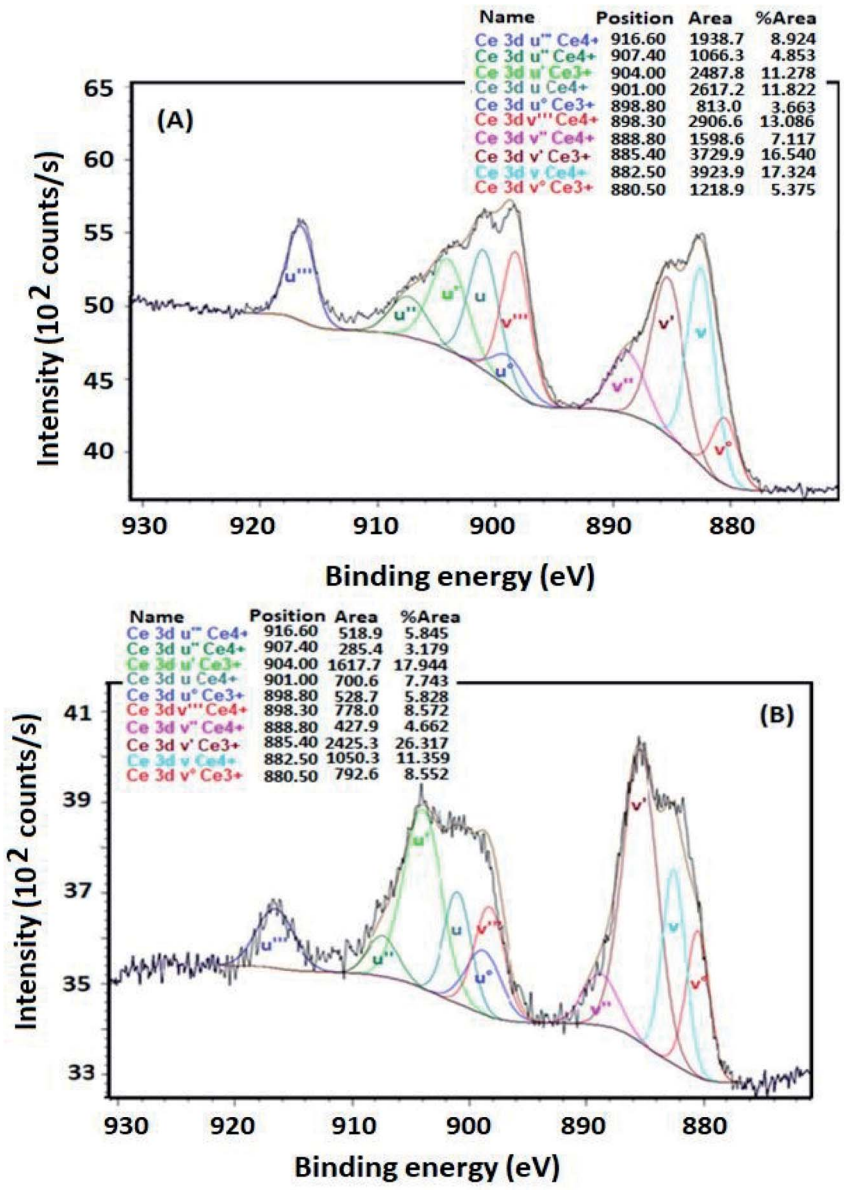

Fig. 5 Ce 3d XPS profile of samples treated at 500 °C, (A) Ce 3d XPS profile of VTiCe catalyst, (B) Ce 3d XPS profile of VTiCeZr catalyst.

dispersed VO_x species.[44,45] It is clear that the incorporation of zirconium affects the reduction behavior of vanadium species. Especially, the reducibility of vanadium becomes more important in the VTiCeZr solid than that of VTi and VTiZr materials since TPR reduction peaks shifted toward lower temperature. These observations suggest that the presence of zirconium species enhance the reduction ability of catalysts. Thus, the VTiCeZr material with better reducibility could indicate better oxygen absorbing capacity and hence could lead to a better catalytic performances.

After ceria addition, a new peak centered at 548 °C appeared in the TPR profile of the V_2O_5/TiO_2–CeO_2 which can be attributed to the reduction of surface Ce^{4+} to Ce^{3+}.[46]

For ZrO_2 containing materials, peaks revealed at 584 °C and 578° for VTiZr and VTiCeZr respectively, could be attributed to the reduction of ZrO_2.[47]

The TPR profile of VTiCeZr catalyst exhibits two peaks around 638 °C and 692 °C which are attributed to the reduction of bulk CeO_2.[48,49] The reduction temperatures are lower than that of CeO_2 (above 700 °C[49,50]). This was associated with the ZrO_2 ability to modify sublattice oxygen into CeO_2–ZrO_2 mixed oxides, generating defective structures and highly mobile oxygen atoms.[49,51]

Combined with the XPS results, the good reducibility owing to the increase of the amount and the kinds of reactive oxygen species can provide a facile redox process that could contribute to enhancing the catalytic activity.

3.7 Catalytic test

The catalytic investigation was performed in the total oxidation of chlorobenzene in order to probe the ability of the prepared

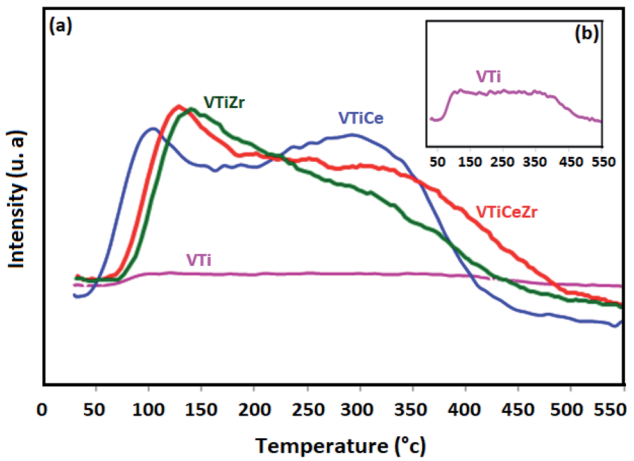

Fig. 6 NH_3-TPD profiles of catalysts treated at 500 °C: (a) NH_3-TPD of VTi, VTiCe, VTiZr and VTiCeZr, (b) NH_3-TPD of VTi.

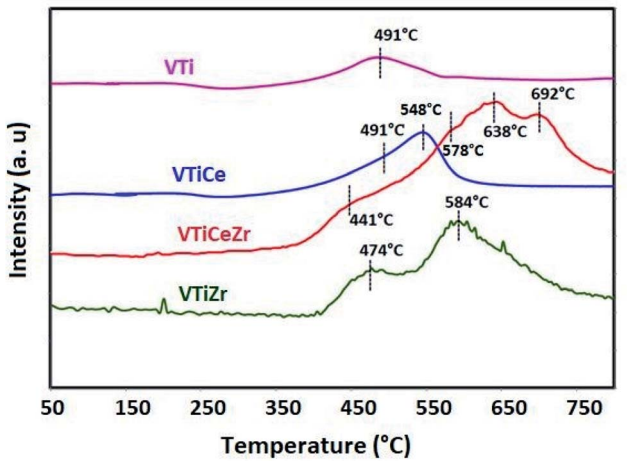

Fig. 7 H_2-TPR profiles of VTi, VTiCe, VTiZr and VTiCeZr samples treated at 500 °C.

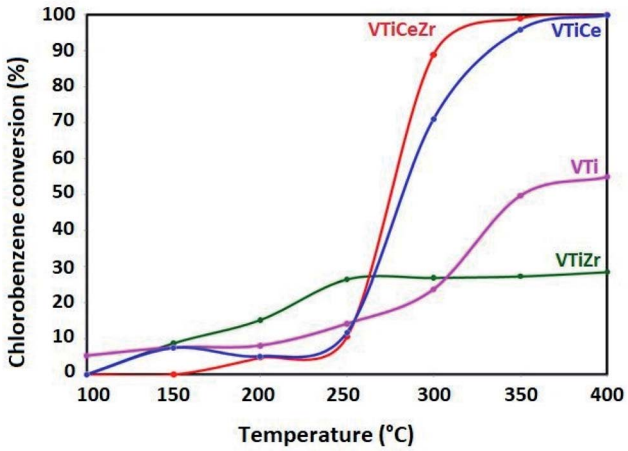

Fig. 8 Chlorobenzene conversion over vanadia supported catalysts.

catalysts to convert chlorobenzene without deactivation. Fig. 8 presents the chlorobenzene light-off curves of the impregnated catalysts supported on TiO_2, TiO_2–CeO_2, TiO_2–ZrO_2 and TiO_2–CeO_2–ZrO_2 in the range 100–400 °C by steps of 50 °C. The reaction was run from 100 °C to 400 °C by steps of 50 °C. At each temperature investigated, the catalyst was stabilized for 150 min in order to reach the steady state. CO_2 is the main product. The carbon balance is completed with carbon monoxide, which is also produced especially at a relatively high temperature (from a few % up to *ca.* 30%). No other partial oxidation products (chlorinated or not) are observed. These observations hold for all the catalysts.

The VTi reference catalyst is almost inactive up to 250 °C. However, it exhibits moderate activity above 300 °C and merely reaches 55% at 400 °C. The incorporation of zirconia into this catalyst brings a slight improvement in catalytic activity in the range (100–250 °C). This improvement could be attributed to (i) the better acidic properties, as shown by NH_3-TPD results, which help the adsorption of the pollutant and/or (ii) the stabilization of the V_2O_5 active phase in a higher oxidation state, as demonstrated by XPS results. Moreover, the superior activity of the V_2O_5/TiO_2 catalyst in the range (300–400 °C) could be related to the higher V surface concentration in VTi sample than that shown by VTiZr as demonstrated by XPS results.

On the other hand, the V_2O_5–TiO_2–CeO_2 and V_2O_5–TiO_2–CeO_2–ZrO_2 catalysts hardly convert chlorobenzene below 250 °C and their activities increase with temperature to reach 100% conversion at 400 °C. However, their behavior with the increase of temperature is quite different. Especially, at 300 °C VTiCeZr catalyst converts 89% while VTiCe converts 71%. This observation pointed up the beneficial effect of the introduction of zirconium groups into the binary oxide TiO_2–CeO_2 aerogel support. In particular, according to XPS results, it seems that zirconia succeeds to stabilize vanadium at a higher oxidation state (V^{5+}). In fact, in the case of VTiCeZr catalyst, ceria mainly exists in the form of Ce^{3+}. The enrichment of Ce^{3+} could create a charge imbalance, and more oxygen vacancies are formed. This could facilitate the activation and transportation of active oxygen species. Indeed, CeO_2 is a powerful oxidant for the regeneration of the V_2O_5 reduced sites. This higher oxidation strength of CeO_2 assisted by ZrO_2 induces a speeding up of the Mars and van Krevelen mechanism.[52] This speeding up corresponds to the observed increase of the chlorobenzene conversion. This result correlates well with that obtained by H_2-TPR. Particularly, VTiCeZr catalyst with better reducibility is the most active catalyst.

4. Conclusion

Our results revealed that Zr-doped V_2O_5 based catalyst is beneficial for the improvement of catalytic properties in chlorobenzene total oxidation. In particular, in the absence of cerium groups, this beneficial effect is in the range (100–250 °C) and it is essentially correlated with the better acidic properties or/and the stabilization of the V_2O_5 active phase in a higher oxidation state. However, in the case of cerium rich catalyst, this positive effect is much stronger. In fact, ZrO_2 increases the

oxygen mobility in the lattice, which, in turn, enhances the redox properties of V_2O_5/TiO_2–CeO_2–ZrO_2 and induces an increase in the chlorobenzene conversion, especially from 300 °C.

Conflicts of interest

There are no conflicts to declare.

References

1 C. Gannoun, R. Delaigle, P. Eloy, D. P. Debecker, A. Ghorbel and E. M. Gaigneaux, *Catal. Commun.*, 2011, **15**, 1–5, DOI: 10.1016/j.catcom.2011.08.001.
2 Y. Yang, H. Li, S. Zhang, X. Yu, S. Liu, R. Qu and C. Zheng, *Catal. Today*, 2020, **355**, 349–357, DOI: 10.1016/j.cattod.2019.11.009.
3 R. Delaigle, D. P. Debecker, F. Bertinchamp and E. M. Gaigneaux, *Top. Catal.*, 2009, **52**(5), 501–516, DOI: 10.1007/s11244-009-9181-9.
4 D. P. Debecker, R. Delaigle, K. Bouchmella, P. Eloy, E. M. Gaigneaux and P. H. Mutin, *Catal. Today*, 2010, **157**(1–4), 125–130, DOI: 10.1016/j.cattod.2010.02.010.
5 C. Du, S. Lu, Q. Wang, A. G. Buekensa, M. Nia and D. P. Debecker, *Chem. Eng. J.*, 2018, **334**, 519–544, DOI: 10.1016/j.cej.2017.09.018.
6 S. H. Taylor, C. S. Heneghan, G. J. Hutchings and I. D. Hudson, *Catal. Today*, 2000, **59**, 249–259, DOI: 10.1016/S0920-5861(99)00162-5.
7 V. De Jong, M. K. Cieplik, W. A. Reints, F. Fernandez-Reino and R. Louw, *J. Catal.*, 2002, **211**, 355–365, DOI: 10.1016/S0021-9517(02)93762-0.
8 C. Gannoun, R. Delaigle, D. P. Debecker, P. Eloy, A. Ghorbel and E. M. Gaigneaux, *Appl. Catal. A: Chem.*, 2012, **447–448**, 1–6, DOI: 10.1016/j.apcata.2012.08.034.
9 B. Murugan and A. V. Ramaswamy, *J. Am. Chem. Soc., J. Am. Chem. Soc.*, 2007, **129**, 3062–3063, DOI: 10.1016/j.apcata.2012.08.034.
10 C. T. Campbell and C. H. F. Peden, *Science*, 2005, **309**, 713–714, DOI: 10.1126/science.1113955.
11 B. M Reddy, A. Khan, Y. Yamada, T. Kobayashi, S. Loridant and J. C. Volta, *J. Phys. Chem. B*, 2003, **107**, 5162–5167, DOI: 10.1021/jp0344601.
12 Y. Nagai, T. Yamamoto, T. Tanaka, S. Yoshida, T. Nonaka, T. Okamoto, A. Suda and M. Sugiura, *Catal. Today*, 2002, **74**, 225–234, DOI: 10.1016/S0920-5861(02)00025-1.
13 J. Kaspar and P. Fornasiero, *Catal. Sci. Ser.*, 2002, **2**, 217–241, http://hdl.handle.net/11368/1687483.
14 Y. Zhang, L. Wang, J. Li, H. Zhang, H. Xu, R. Xiao and l. Yang, *Chinese J. Catal.*, 2016, **37**, 1918–1930, DOI: 10.1016/S1872-2067(16)62510-X.
15 E. H-Ramírez, J. A. Wang, L. F. Chen, M. A. Valenzuela and A. K. Dalai, *Appl. Surf. Sci.*, 2017, **399**, 77–85, DOI: 10.1016/j.apsusc.2016.12.068.
16 J.-M. Giraudon, T. B. Nguyen, G. Leclercq, S. Siffert, J.-F. Lamonier, A. Aboukaıs, A. Vantomme and B.-L. Su, *Catal. Today*, 2008, **137**, 379–384, DOI: 10.1016/j.cattod.2008.02.019.
17 H. L. Tidahy, S. Siffert, J.-F. Lamonier, E. A. Zhilinskaya, A. Aboukaıs, Z.-Y. Yuan, A. Vantomme, B.-L. Su, X. Canet, G. De Weireld, T. B. N'Guyen, J.-M. Giraudon and G. Leclercq, *Appl. Catal. A: Gen.*, 2006, **310**, 61–69, DOI: 10.1016/j.apcata.2006.05.020.
18 C. Liu, Y. Bi and J. Li, *Appl. Surf. Sci.*, 2020, **528**, 146695, DOI: 10.1016/j.apsusc.2020.146695.
19 Y. Zhang, X. Yue, T. Huang, K. Shen and B. Lu, *Materials*, 2018, **11**, 1307, DOI: 10.3390/ma11081307.
20 S. Palma Del Valle, O. Marie and H. P. Nguen, *Appl. Catal., B*, 2018, **223**, 116–124, DOI: 10.1016/j.apcatb.2017.02.053.
21 B. M Reddy and A. Khan, *Rev. Sci. Eng.*, 2005, **47**, 257–296, DOI: 10.1081/CR-200057488.
22 *Degussa Technical Bulletin Pigment Report*, 1990, vol. 56, p. 13.
23 B. M. Reddy, P. Lakshmanan and A. Khan, *J. Phys. Chem. B*, 2005, **109**, 1781–1787, DOI: 10.1021/jp045723+.
24 IUPAC, *Pure and Appl. Chem.*, 1985, **57**, 603–619, DOI: 10.1351/pac198557040603.
25 H. Imagawa, T. Tanaka, N. Takahashi, S. Matsunaga, A. Suda and H. Shinjoh, *J. Catal.*, 2007, **251**, 315–320, DOI: 10.1016/j.jcat.2007.08.002.
26 H. Imagawa and H. Imagawa, *R&D Rev. Toyota CRDL*, 2011, **42**, 63–70, https://www.tylabs.co.jp.review.
27 C. Gannoun, A. Turki, H. Kochkar, R. Delaigle, P. Eloy, A. Ghorbel and E. M. Gaigneaux, *Appl. Catal., B*, 2014, **147**, 58–64, DOI: 10.1016/j.apcatb.2013.08.009.
28 B. Yang, Y. Shen, S. Shen and S. Zhu, *J. Rare Earths*, 2013, **31**, 130–136, DOI: 10.1016/S1002-0721(12)60246-4.
29 M. Li, S. Zhang, L. Lv, M. Wang, W. Zhang and B. Pan, *Chem. Eng. J.*, 2013, **229**, 118–125, DOI: 10.1016/j.cej.2013.05.106.
30 K. N. Rao and B. M. Reddy, *Appl. Catal., B*, 2010, **100**, 472–480, DOI: 10.1016/j.apcatb.2010.08.024.
31 C. Gannoun, R. Delaigle, A. Ghorbel and E. M. Gaigneaux, *Catal. Sci. Technol.*, 2019, **9**, 2344–2350, DOI: 10.1039/c9cy00099b.
32 J. Wang, Y. Yu, S. Li, L. Guo, E. Wang and Y. Cao, *J. Phys. Chem. C*, 2013, **117**, 27120–27126, DOI: 10.1021/jp407662d.
33 Z. Li, J. Li, S. Liu, X. Ren, J. Ma, W. Su and Y. Peng, *Catal. Today*, 2015, **258**, 11–16, DOI: 10.1016/j.cattod.2015.07.002.
34 M. A. Larrubia, G. Ramis and G. Busca, *Appl. Catal., B*, 2000, **27**, L145–L151, DOI: 10.1016/S0926-3373(00)00150-8.
35 G. Silversmit, D. Depla, H. Poelman, G. B. Marin and R. De Gryse, *J. Electron Spectrosc. Relat. Phenom.*, 2004, **135**, 167–175, DOI: 10.1016/j.elspec.2004.03.004.
36 S. Chin, S.-E. Park, M. Kim, G. N. Bae and J. Jurng, *Powder Technol.*, 2012, **217**, 388–393, DOI: 10.1016/j.powtec.2011.10.055.
37 B. M. Reddy, K. N. Rao, G. K. Reddy, A. Khan and S.-E. Park, *J. Phys. Chem. C*, 2007, **111**, 18751–18758, DOI: 10.1021/jp076617l.
38 B. M. Reddy, P. Bharali, P. Saikia, A. Khan, S. Loridant, M. Muhler and W. Grunert, *J. Phys. Chem. C*, 2007, **111**, 10478–10483, DOI: 10.1021/jp071485h.
39 W. Shan, Y. Geng, Y. Zhang, Z. Lian and H. He, *Catalyst*, 2018, **8**(12), 1–12, DOI: 10.3390/catal8120592.

40 L. Chmielarz, P. Kustrowski, M. Zbroja, W. Lasocha and R. Dziembaj, *Catal. Today*, 2004, **90**, 43–49, DOI: 10.1016/j.cattod.2004.04.007.

41 S. S. R. Putluru, L. Schill, A. Godiksen, R. Poreddy, S. Mossin, A. D. Jensen and R. Fehrmann, *Appl. Catal., A*, 2016, **183**, 282–290, DOI: 10.1016/j.apcatb.2015.10.044.

42 J. Arfaoui, L. Khalfallah Boudali, A. Ghorbel and G. Delahay, *Catal. Today*, 2009, **142**, 234–239, DOI: 10.1016/j.cattod.2008.07.032.

43 R. Delaigle, D. P. Debecker, F. Bertinchamps and E. M. Gaigneaux, *Top. Catal.*, 2009, **52**, 501–516, DOI: 10.1007/s11244-009-9181-9.

44 H. Poelman, B. F. Sels, M. Olea, K. Eufinger, J. S. Paul, B. Moens, I. Sack, V. Balcaen, F. Bertinchamps, E. M. Gaigneau, P. A. Jacobs, G. B. Marin, D. Poelman and R. De Gryse, *J. Catal.*, 2007, **245**, 156–172, DOI: 10.1016/j.jcat.2006.09.022.

45 G. Y. Popova, T. V. Andrushkevich, E. V. Semionova, Y. A. Chesalov, L. S. Dovlitova, V. A. Rogov and V. N. Parmon, *J. Mol. Catal. A: Chem.*, 2008, **283**, 146–152, DOI: 10.1016/j.molcata.2007.12.019.

46 Z. Lian, F. Liu and H. He, *Ind. Eng. Chem. Res.*, 2014, **53**, 19506–19511, DOI: 10.1021/ie504188s.

47 D. Pakhare, H. Wu, S. Narendra, V. Abdelsayed, D. Haynes, D. Shekhawat, D. Berry and J. Spivey, *Appl. Petrochem. Res.*, 2013, **3**, 117–129, DOI: 10.1007/s13203-013-0042-x.

48 A. Trovarelli, F. Zamar, J. Llorca, C. Leitenburg, G. Dolcetti and J. T. Kiss, *J. Catal.*, 1997, **169**, 490–502, DOI: 10.1006/jcat.1997.1705.

49 M. A. Ebiad, D. R. Abd El-Hafiz, R. A. Elsalamony and L. S. Mohamed, *RSC Adv.*, 2012, **2**, 8145–8156, DOI: 10.1039/c2ra20258a.

50 R. O. da Fonseca, A. A. A. da Silva, M. R. M. Signorelli, R. C. Rabelo-Neto, F. B. Noronha, R. C. C. Simões and L. V. Mattos, *J. Braz. Chem. Soc.*, 2014, **25**, 2356–2363, DOI: 10.5935/0103-5053.20140245.

51 L. Meng, L. Liu, X. Zi, H. Dai, Z. Zhao, X. Wang and H. He, *Front. Environ. Sci. Eng. China*, 2010, **4**, 164–171, DOI: 10.1007/s11783-010-0019-2.

52 P. Mars and D. W. Van Krevelen, *Chem. Eng. Sci.*, 1954, **3**, 41–59, DOI: 10.1016/S0009-2509(54)80005-4.